Chinese Chemical Letters 34 (2023) 107623

Contents lists available at ScienceDirect

Chinese Chemical Letters

journal homepage: www.elsevier.com/locate/cclet

Rationally designed amyloid inhibitors based on amyloid-related structural studies

Jinjian Hu[a], Yufen Zhao[a,d], Yanmei Li[a,b,c,*]

[a] Department of Chemistry, Key Lab of Bioorganic Phosphorus Chemistry & Chemical Biology, Tsinghua University, Beijing 100084, China
[b] Beijing Institute for Brain Disorders, Beijing 100069, China
[c] Center for Synthetic and Systems Biology, Tsinghua University, Beijing 100084, China
[d] Institute of Drug Discovery Technology, Ningbo University, Ningbo 315221, China

ARTICLE INFO

Article history:
Received 20 March 2022
Revised 15 June 2022
Accepted 19 June 2022
Available online 24 June 2022

Keywords:
Amyloid
Amyloid structure
Degenerative disease
Amyloid inhibitor
Rational design

ABSTRACT

Amyloid proteins correlate with a series of degenerative diseases. Targeting amyloid aggregation has remained a hot topic in therapeutic studies. Numerous inhibitors have been developed, but very few have been approved for marketing. Meanwhile, the growing knowledge of amyloid structural characteristics provides a basis for the rational design of inhibitors. Here we introduce the high-resolution structural findings of amyloid fibrils in recent years and discuss the reported strategies toward rationally designed inhibitors based on amyloid-related structural studies.

1. Introduction

Amyloidogenic proteins are a type of protein which can misfold and form aggregates or even fibrils with cross-β structure. These aggregates in diseased tissue are believed to be the hallmarks of multiple degenerative diseases, including Alzheimer's disease (AD), Parkinson's disease (PD), type 2 diabetes (T2D), amyotrophic lateral sclerosis (ALS), prion protein (PrP) related diseases, and many other amyloidoses [1]. Some states of these aggregates are believed to be harmful to the living cell, including the toxic oligomer of multiple proteins [2–5] and the relatively inert fibrils, which may cause membrane disruption, and occupy space in cells [6,7]. Moreover, the amyloid fibrils show prion-like properties. In other words, the misfolded amyloid protein can influence the normal proteins, convert them into misfolded forms that can be transmitted to neighboring cells, leading to the "progressive disorder" [8–11].

As a consequence, targeting amyloid aggregation is a hot topic for therapy. Numerous inhibitors targeting this process have been developed and tested. Screens have been developed and run to identify compounds that stabilize monomers, prevent seeding, disassociate fibrils, form fewer toxic aggregates and target aggregation-related posttranslational modifications [12–14]. However, only one amyloid inhibitor targeting transthyretin, whose aggregation leads to systemic amyloidosis, has been approved for marketing [15].

A likely reason for the limited success of these screens is the use of nonideal target among the amyloid self-assembly states. The process of amyloid self-assembly is commonly described as a four-step process, including primary nucleation, secondary nucleation, fibril elongation, and fibril fragmentation [16]. Initially, most aggregation inhibitors targeted the elongation or disrupted the fibril. Although fibrils are the hallmarks of amyloidosis, low-molecular-weight oligomers have emerged as more toxic species [2–4]. These discoveries partially explain the failure of these inhibitors, as oligomers are more easily to form and lead to toxicity and inflammation in these strategies. In addition, unlike transthyretin, most amyloidogenic proteins are unfolded in solution and contain intrinsically disordered regions (IDRs), leading to difficulties in stabilizing the monomer state. Selectivity and bioavailability are also problems, especially for some small molecule inhibitors, such as curcumin [17,18].

With the growing knowledge of amyloids, rationally designed inhibitors have become an attractive choice. However, there are some limitations, which include the lack of defined target structures, many similar assembly species, large and variable surfaces,

* Corresponding author at: Department of Chemistry, Key Lab of Bioorganic Phosphorus Chemistry & Chemical Biology, Tsinghua University, Beijing 100084, China.
E-mail address: liym@mail.tsinghua.edu.cn (Y. Li).

https://doi.org/10.1016/j.cclet.2022.06.046
1001-8417/

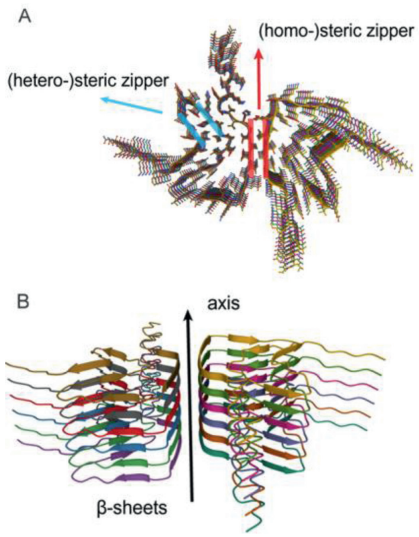

Fig. 1. Cryo-EM structure of an α-synuclein fibril polymorph, showing the steric zippers in amyloid filaments. Image from the RCSB PDB (rcsb.org), PDB entry: 6A6B [25], DOI citation: 10.2210/pdb6a6b/pdb.

low concentrations of substrate proteins, and specific property requirements for drugs, such as solubility, stability and blood–brain barrier permeability [19]. In recent years, with the development of improved structure determination methods, especially cryoelectron microscopy (cryo-EM) and solid-state NMR (ssNMR), high-resolution structures of amyloid fibrils have become available. These data help to elucidate the molecular basis of amyloid polymorphism [20,21] and provide more information for the design of structure-based inhibitors. Quite a few inhibitors have been developed with a structural basis and have shown satisfactory inhibition (Fig. 3).

Here we review the high-resolution structures of amyloid fibrils found in recent years and discuss the design strategies of inhibitors targeting fibrils. We assume that these new discoveries in fibril structures will inspire the development of more potential inhibitors.

2. High-resolution structures of amyloids

Though having differences in length and sequence, amyloid proteins share a similar unbranched cross-β fibril structure [20]. The monomers in one sheet stack along the axis and are parallel or antiparallel with each other. One or more of these stacked sheets make up a protofilament. They tightly bind together with the side chains of each monomer in the same layer interdigitating [20]. This structure resembles a zipper in the cross section, thus it is also called a steric zipper (Fig. 1). Usually at least two protofilaments form a fibril. Due to the weak noncovalent interactions, the binding style of the sheets and the number of protofilaments in fibrils vary, which contributes to polymorphism in the amyloid structure. And the polymorphs may be related to the conception of strains in diseases.

Despite the knowledge of common structural characteristics, it is challenging to understand the differences in polymorphs. Thus high-resolution structures are in need. In recent years, ssNMR and cryo-EM have been concentrated and well-developed [22,23]. Compared with other methods, like X-ray and electron diffraction, there is no need for the preparation of large crystals, which facilitates the structural analysis of more proteins. Usually, ssNMR gives a model that satisfies the constraints of the residues and side chain interactions according to the detected signals. The more constraints are determined, the more reliable and clearer the final model will be. Nevertheless, cryo-EM has more advantages in the determination of polymorph structures. Although cryo-EM usually has lower resolution than X-ray diffraction in resolution and requires larger instruments and complex computational approaches, it can give more information about fibrils and uniquely identify multiple polymorphs in one data collection (if these polymorphs exist in the same collection), whereas usually only one structure of homosteric zippers can be obtained in X-ray diffraction [20,24]. Besides, cryo-EM directly reveals the positions of residues and side chains, which avoids the argument of possible models in ssNMR. It also has advantages in dealing with the structure of large proteins, since the modelling process will be much more complicated in ssNMR with too many restraints. Moreover, when analyzing the fibrils from patient samples, cryo-EM is more suitable, as ssNMR requires additional seeding and elongation process in isotopically labelled monomers, which takes more time and isa less direct measurement. However, the long data collection time and complicated condition optimization for sample preparation restrict its application.

Recently, ssNMR and cryo-EM have both been used to reveal amyloid fibril structures. And we will introduce these findings below.

2.1. Aβ

Aβ is a series of polypeptides derived from amyloid precursor protein (APP). Due to the cleavage sites of γ-secretase and β-secretase, the final length of Aβ varies between 39 and 43. The most common form in brain is Aβ_{40}, however, Aβ_{42} is believed to be more toxic and more prone to aggregate [26].

During 2005–2008, two models of fibrils of synthesized Aβ_{40} were determined by ssNMR in Tycko's group [27–29]. These structures both belong to Aβ_{40}, but appear distinctly different. The number of seeding rounds and fibril growth conditions influence the final polymorph. These two models both have U-shaped arms in residues 10–22 and 30–40. But the final protofibril can be a dimer with 2-fold symmetry or a trimer with 3-fold symmetry. Later in 2015, Böckmann, Glockshuber, Meier and co-workers also provided a model [30]. This model described Aβ_{40} fibrils with the Osaka deletion mutation E22Δ. It showed a different dimer with no U-shaped arm, but a "cinnamon roll" with C-terminus packed in the center. The mutant site is in a unique turn within the structure, and close to other familial mutant sites, indicating that this structure is accessible to Aβ_{40} and related mutants [30].

Compared with Aβ_{40}, the fibril structure of Aβ_{42} has attracted more attention. As described, Aβ_{42} seems directly related to plaques in patients' brains [31,32]. The additional two residues accelerate aggregation compared with Aβ_{40}. In 2015, Ishii and coworkers presented a single-filament model of Aβ_{42} by ssNMR [33]. The monomer adopts a triple parallel-β-sheet form, like the inverted S-shape. Then in 2016, Griffin's group, Böckmann, Glockshuber and Meier's collaborative team presented a same model of A$\beta_{42,}$ respectively [31,34]. A dimer containing two S-shaped monomers was described in this model. Compared with the previous monomer model, the dimer model has a homosteric zipper near the axis. It is noticeable that this model partially explained the difference in aggregation rate between Aβ_{40} and Aβ_{42}. Compared with Aβ_{40}, the Aβ_{42} fibril model has a distinct hydrophobic patch composed of V40 and A42, which corresponds with the previous hypothesis that Aβ_{42} is more hydrophobic than Aβ_{40}.

High-resolution structure of Aβ fibrils was also determined by cryo-EM. Early in 2006, Grigorieff and Fändrich's team first used cryo-EM to analyze the structure of Aβ_{40} fibrils and obtained a density map with a resolution of only 26 Å [35]. Then in 2008, they presented an about 8 Å-resolution structure of Aβ_{40} fibrils by

mass-per-length (MPL) and cryo-EM with developed image processing tools [36]. Despite the great progress in resolution, it is impossible to see the residue positions. Only a local two-fold symmetric structure with some U-shaped area can be affirmed. They also constructed the model of Aβ_{42} and made a comparison of Aβ_{40} and Aβ_{42} in 2009 [37]. Another 13 nm-wide Aβ_{40} fibril which is different from the 20 nm-wide fibril in previous work was also captured. The comparison showed different structures of Aβ_{40} and Aβ_{42}, but the resolution was insufficient. In the same year, Frieden and co-workers established a model of Aβ_{42} with a resolution of 10 Å [38]. They noticed a hollow core in the center of the dimer's axis, which corresponded with previous ssNMR results. However, in their observation, each monomer takes the U-shaped instead of the S-shaped form. This finding does not conflict with previous findings because of the polymorph phenomenon in amyloid fibrils.

With the development of cryo-EM and 3D reconstruction, in 2015, Grigorieff and Fändrich's team reported a distinct model of Aβ_{42} with the help of helical reconstruction software [39]. This model showed a dimer with an overall resolution of 7 Å. Though the resolution remains insufficient, especially in the peripheral domains of this model, the researchers used "restraint-driven molecular modelling" to ensure that the core structure is accurate. They even analyzed the steric zippers of Aβ in the Protein Data Bank and the ZipperDB database. They found a fitted structure with the same six residues predicted in this model. Overall, this model described a core region consisting of two tilde-shaped leaflets. The residues 31–36 form one leaflet. And the N-terminal peripheral region extends and wraps the core region.

In 2017, Willbold and Schröder's team reported a structure of Aβ_{42} fibrils containing two intertwined protofilaments by cryo-EM with 4 Å resolution [40]. They also referred to ssNMR and X-ray diffraction results as the argument of this model. A distinct LS-shaped structure of the cross section was revealed with the N-terminal region resembling "L", and the C-terminal region resembling "S". The whole fibril is approximately 2_1 screw symmetric instead of C2 symmetric, which may lead to a different growth pathway from before. In addition, the residues 20–25 form a different turn, which may explain some familial mutants.

Fibrils from patient samples have also been studied. In 2019, Fändrich and co-workers analyzed the Aβ_{40} fibrils purified from 3 patients' brain tissues [41]. They found right-handed twisted fibrils and identified the 3 most abundant polymorphs. This finding was sharply distinct from the *in vitro* left-handed findings. In this model with 4.5 Å resolution, morphology I was a dimer. The cross section of each stack in this dimer takes a C-shaped form. The N-terminal and C-terminal regions fold back onto the central domain. And the central domain of each peptide, especially the residues 24–26, is buried in the fibril core. It seems that morphology II and III are the dimer and trimer of morphology I, respectively in the cross section. These two polymorphs share the same interface formed by Glu3 and Arg5 due to their charges. Cryo-EM structures of Aβ_{42} filaments from human brains were also analyzed recently [42]. Two polymorphs from 10 individuals were identified. These two polymorphs both have a left-handed twist but differ from previous studies. Two S-shaped folds appear in both polymorphs but form interfaces with opposite sides. Although many previous structures of Aβ_{40} or Aβ_{42} fibrils revealed some S-shaped structures, none of the Aβ_{42} filaments takes similar side chain orientations and contacts or the same interfaces. Only an ssNMR structure of the Aβ_{40} E22Δ fibril is similar to one of the polymorphs [30].

2.2. Tau

Tau protein is another disease-related protein in Alzheimer's disease, which was the main component of neurofibrillary tangles (NFTs). It has 6 isoforms in humans due to alternative mRNA splicing. The longest isoform 2N4R contains 441 residues. Thus it is difficult to reveal a full-length model by ssNMR. Previous studies mainly focused on the fragment structures of tau, including the VQIVYK sequence [43], the proline-rich region P2 [44], and K19, a fragment of 2N3R tau [45,46]. However, fibril structure of full-length tau was not available.

These years, cryo-EM has been used to fill this gap. In 2017, Goedert and Scheres's team presented cryo-EM maps of tau in an AD patient at 3.4–3.5 Å resolution and proposed a model of tau paired helical filaments (PHF) and straight filaments [47]. In 2018, they further explored the tau filament structure in different patients [48]. They determined the tau filament structure in an additional 3 patients by cryo-EM, and analyzed the tau morphologies in all these 4 patients and 13 other patients with different types of AD with immuno-gold negative-stain electron microscopy (immuno-EM). They found that the PHFs and SFs in these cases share a common cross-β/β-helix C-shaped core architecture. The structural models of tau PHF and SF were at about 3.2 Å and 3.3 Å, respectively. And they showed a dimer of double-layered C-shaped folded core of R3, R4 regions and additional 10–12 residues. Other residues are fuzzy around this core.

Tau inclusion exists not only in AD, but also in a series of diseases, such as Pick's disease (PiD), progressive supranuclear palsy (PSP), chronic traumatic encephalopathy (CTE) and corticobasal degeneration (CBD). The main isoforms in the inclusions of these diseases are different. In AD and CTE, all isoforms are incorporated into filaments, whereas in PiD, only 3R isoforms are involved. The filaments of PSP and CBD only contain 4R tau. The structures of tau filaments in these diseases also differ slightly. Goedert and Scheres's team performed a series structure determination of tau filaments [49–51]. They obtained two types of tau filament cores in 3 CTE patients. Both of them are dimers of C-shaped tau filaments with more open fold. The only difference is the interfaces of these two dimers. Besides, they noticed extra density in the cavity of the double-layer C-shaped filament, indicating a hydrophobic molecule filled in this cavity. The tau filaments in PiD are quite different. There were two types—the narrow filament and the wide filament. The wide filament core is a dimer of the narrow ones. And the narrow one is a J-shaped filament in the cross section, formed by R1, R3 and R4 regions of tau. This model may explain why only 3R tau is present in Pick body, as the fibril template of 3R tau has an omega-like structure formed by residues 270–273, which cannot accommodate β-branched residues, like V300 in 4R tau. The fibril core of tau in CBD is much more compact. It contains the last residue of R1, whole R2, R3 and R4, and 12 residues after R4. The core takes a unique four-layer conformation, with a hydrophilic cavity, which is opposite from what is seen in CTE core. The authors also provided an explanation for why only 4R tau exists in CBD. In short, it is because some residues in the R1 region in 3R tau do not fit the fibril template in CBD. More recently, Petrucelli and Fitzpatrick's team also reported some tau polymorphs from the brain tissue of patients with CBD and AD [52]. In addition to the structure models, they discussed the potential role of posttranslational modifications such as acetylation and ubiquitination and gave the density maps of ubiquitinated tau, which directly showed how ubiquitination influences fibril structure.

These fibril models in patients seemed to share a similar core fold in individuals with the same disease. However, the *in vitro* tau filament showed polymorphisms similar to Aβ in cryo-EM. Goedert and Scheres's team determined the structure of heparin-induced tau filaments by cryo-EM [53]. Four filaments in different shapes were observed, including snake filaments, twister filaments, jagged filaments, and a dimer of 2N3R filaments. Although these filaments obviously differ from the filaments in patient tissue, they may help

to understand some aggregation processes of tau, for example, the aggregation with polyanionic molecules, such as RNA.

2.3. α-Syn

α-Synuclein (α-syn) is a protein with 140 residues. And it was found to be the main component of Lewy bodies in Parkinson's disease. α-Syn is also associated with dementia with Lewy bodies and multiple system atrophy (MSA). To some extent, α-syn is similar to tau due to their central role in multiple amyloidoses. According to ssNMR studies [54–56], the α-syn fibril is formed by one stack of monomers with winding β-sheets and has a unique Greek-key β-sheet in the cross section.

Recently, the high-resolution structure of α-syn fibrils has attracted the attention of researchers. In 2018, Stahlberg's group determined the structure of α-syn 1–121 fibrils with cryo-EM [57]. They proposed a model of α-syn 38–95 with an overall resolution of 3.4 Å. The fibril in this model contains 2 filaments with a screw symmetry of 2_1. Residues 51–56 in each stack of monomers form the interface of the steric zipper. Compared with the NMR model, the orientation of A53 is different. In this model, the side chain of A53 points to the interface of steric zippers, which may contribute to fibril stability. Liu and Li's team also explored the structure of α-syn fibrils, in 2018, they analyzed the fibrils of N-terminal acetylated recombinant full-length α-syn 1–140 [25]. They obtained a density map with an overall resolution of 3.07 Å. Then they built a model of residues 37–99. This model is a twisted dimer of two stacks of monomers. Similar to Stahlberg's model, the dimer is left-handed. Each stack of monomers contains a Greek-key-like structure similar to the previous NMR study [54]. In the same year, Eisenberg, Boyer and Jiang's collaboration team proposed another 2 models of full-length α-syn fibrils [58]. One polymorph has a twist in its projection views, therefore called "twister", whereas the other lacks an apparent twist, called "rod". Both of these fibrils are left-handed and share a similar core at residues 50–77. However, the interfaces of the filaments in these two polymorphs are different. In the twister structure, the interface between two protofilaments is a homosteric zipper of NACore (residues 68–78), whereas the rod polymorph packs around the preNAC region (residues 47–56), which contains some familial mutation sites (E46K, H50Q, G51D, A53E, A53T and A53V). Since these mutation sites are not involved in the NACore, it suggests that the disease-related mutant may interfere the formation of rod polymorph. And this was proved in the studies of mutant α-syn fibrils, including E46K [59–61], H50Q [62] and A53T [63]. Consistent with this hypothesis, the fibril structures in these studies are different from those of wild-type, but the kernel region of residues 50–77 is still similar in these structures [62]. Later in 2019, Stahlberg's group collaborated with Böckmann and Bousset's group analyzed the full-length α-syn fibrils [59]. They further improved the resolution (2.99 Å and 3.39 Å) and proposed structures of two new polymorphs. These two structures are different from previously found polymorphs. There is no Greek-key structure or even the kernel of residues 50–77. The different arrangement also leads to different interfaces in these polymorphs. In detail, the interfaces in this study are formed *via* the electrostatic interactions between residues K45 and E57 or E46, whereas the previous interfaces were formed by nonpolar residues.

Besides, the structures of phosphorylated α-syn fibrils have been determined, since the posttranslational modifications of α-syn, especially phosphorylation, are believed to be a disease-related phenomenon in Parkinson's disease [59,64,65]. The position of the phosphorylation site seemed crucial to the structures in these studies. Phosphorylation at tyrosine-39 significantly influenced the structure, whereas the phosphorylation at serine–129, although lacking a clear model, seemed similar to the wild type polymorph. In the model of pY39 α-syn fibrils [64], the entire N terminal region of α-syn is involved in the fibril core, and there is a unique hydrophilic tunnel in the core. This model provided direct evidence that tyrosine-39 phosphorylation interferes with amyloid structure and explained some phenomena, such as the increased toxicity of phosphorylated α-syn in neuron cells and the lower solubility which may even enhance the pathology.

For α-syn, the cryo-EM structure from patient samples was only analyzed in patient with MSA in 2020 [66]. Goedert and Scheres's team identified two polymorphs. Similarly, the polymorphs are distinguished from recombinant fibrils. Besides, non-proteinaceous molecules are also found in this structure, which is also revealed in tau filaments [50,51].

2.4. TDP-43

TAR DNA-binding protein (TDP-43) is a 414-residue protein first found to bind to the transactive response element of HIV-1. It is also involved in transcription and RNA splicing processes. Meanwhile, in amyotrophic lateral sclerosis (ALS) and frontotemporal dementia (FTLD), TDP-43 accumulates in inclusions and is associated with these diseases [67,68]. The C-terminus of TDP-43 mainly consists of the low-complexity domain (LCD) and is thought to play important roles in aggregation.

In 2018, Eisenberg's group used X-ray diffraction and microcrystal electron diffraction to determine the core of fibril. They selected ten short peptide fragments from the TDP-43 LCD sequence in the ZipperDB database [69]. They reported 6 steric zippers formed by these sequences and proposed a mechanism by which these regions act in reversible or irreversible aggregation. Then in 2020, Yang's group used ssNMR and analyzed recombinant C-terminal TDP-43 (274–414) fibrils [70]. They did not propose a complete model, but still revealed some information, including the rigid core of residues 306–343 and 363–397. In 2019, Eisenberg's group tried to apply cryo-EM to structure determination of TDP-43 LCD fibrils [71]. Despite their efforts on condition optimization, they did not obtain a proper sample for cryo-EM with entire LCD. Therefore, they divided the LCD into 2 segments: segment A (residues 311–360) and segment B (residues 286–331). They identified 3 polymorphs of segment A and 1 polymorph of segment B with A315E mutant. Three polymorphs of segment A are similar, and share a dagger-shaped fold at residues 320–334. And the segment B fibrils are formed by two pairs of R-shaped segments.

Recently, Surewicz's group reported a cryo-EM structure of the entire TDP-43 LCD (267–414) fibril [72]. They optimized the pH to about 4 and chose a clear, left-handed fibril for analysis. Finally, they obtained a density map with a nominal resolution of 3.2 Å and built a near-atomic-resolution model of the fibril core. It is noticeable that the fibril core contains 139 residues (residues 276–414), which is the longest sequence of an amyloid core to date. This large core can be divided into two parts. The N-terminus is rich in hydrophobic amino acids and the nonpolar side chains pack with each other to form hydrophobic cores. And the C-terminus contains primarily hydrophilic amino acids.

Although the structure determination of TDP-43 C-terminal fibrils was successful, there was a study showing that TDP-43 fragments of different lengths had different signals in ssNMR, which indicates that the N-terminal and RNA recognition motifs influence the aggregation process [73]. In a recent article, Ryskeldi-Falcon and co-workers reported the cryo-EM structure of pathological TDP-43 fibrils extracted from samples of patients having ALS with FTLD [74]. A double-spiral-shaped fold structure was found. This model is quite different from recombinant TDP-43, both in chirality and secondary structure, which may provide more pathological information for therapy.

2.5. hIAPP

Human islet amyloid polypeptide (hIAPP) is a 37-residue peptide secreted by pancreatic islet β-cells. Under physiological conditions, hIAPP can help modulate glucose levels. However, hIAPP is prone to aggregate and its deposits exist in over 90% of patients with type 2 diabetes, which may lead to membrane disruption and cytotoxicity [75–78]. The structure of hIAPP fibrils was determined early with ssNMR [79,80]. In these studies, the hIAPP fibril was described as a pair of opposing β-sheets (14–19 and 31–36) with a flexible loop linking these two parts. The β-sheets in each layer pack together and form the protofilament.

To provide direct insight into the hIAPP fibril structure, in 2020, Eisenberg's group determined the structure of SUMO-tagged hIAPP fibrils by cryo-EM [81]. They obtained a 3.7 Å-resolution structure of a twisted polymorph. In this map, two protofilaments are related by a *pseudo*-2_1 axis. Each hIAPP adopts a meandering topology. Due to the quasi-symmetrical amino acid sequence of hIAPP and the limited resolution of the map, they proposed 2 possible atomic models. They further developed a capping inhibitor based on this model, which will be introduced in detail in the 3.2 part.

Hoyer and Schröder's team also analyzed 3 polymorphs with cryo-EM [82]. They incubated C-terminal amidated hIAPP at pH 6.0 and found 5 polymorphs. among these polymorphs, only the most abundant polymorph is clear enough for modelling. This polymorph is right-helical and consists of two stacks of S-shaped monomers. Interestingly, this structure is similar to the S-shaped Aβ polymorph [31,34]. And if compared with LS-shaped Aβ, the disease-related mutantation S20G of hIAPP and mutantation E22G of Aβ are located in the similar position. This phenomenon may be due to the sequence similarity of hIAPP and Aβ. The similar structures also help explain the cross-seeding of hIAPP and Aβ [83].

2.6. Prion

Prion protein was found early and its abnormal form PrP-Scrapie (PrP^{Sc})is related to some diseases, such as genetic Creutzfeldt-Jakob disease (gCJD), fatal familial insomnia (FFI) and Gerstmann-Straeussler-Scheinker syndrome (GSS) [84]. The native structure of prion protein was identified in 1996 [85]. However, the structure determination of prion fibrils was hindered due to the insolubility and high heterogeneity of *in vivo* materials. Only a few works have investigated the PrP fibril structure by ssNMR. For example, Jaroniec and co-workers used magic-angle spinning (MAS) ssNMR techniques in analyzing the amyloid core and N-terminal of C-truncated Y145Stop human prion protein [86,87], presenting a model [88], and showing the solvent interfaces of fibrils [89].

Recently, Rodriguez's team gained an atomic structure of recombinant human PrP 94–178 fibrils with cryo-EM [90]. Like other amyloid fibrils, the major fibril polymorph of PrP forms a parallel, in-register structure. However, the fibril core contains two filaments, with 44 nonpolar residues of each filament buried in the fibril core. This uncommon compact structure explained the resistance of PrP to denaturants, proteases and detergents. Liang and Liu's team also applied cryo-EM to PrP fibrils [91]. They prepared recombinant full-length PrP (23–231) fibrils and obtained a different core model of 14 nm in diameter. The 2.7 Å-resolution map showed that the fibril is almost a twisted dimer with a screw symmetry of 2_1. And each protofilament in the dimer is mainly formed by residues 170−229. The two protofilaments in the dimer share a relatively narrow interface from residues 194–196. The C179 and C214 form a disulfide bridge, which helps to stabilize the compact structure. Overall, this model was unique, less compact compared with previous studies.

Besides, the cryo-EM structure of human Y145Stop PrP (23–144) fibrils was also reported [92]. This mutant was believed to be infectious and extensively used as a model for studying prion propagation [88,93]. Surewicz's team presented a 2.86 Å-resolution map of its fibril recently. This model showed an unusual fibril core consisting of four protofilaments. Each subunit contains an S-shaped backbone and assembles through large hydrophobic interfaces. This model indicated the structural differences of fibrils with different truncations, which may explain some questions about propagation and seeding properties of prions.

To date, there have been many clear atomic structure models of amyloids (Table 1). And the resolution of these models has increased in these years. It is easy to notice that many newly identified structures differ from previous ones. The differences partially result from the different protein lengths in the studies. But a more likely cause of discrepancy is the polymorphism of fibrils. The polymorphisms explain certain phenomena, such as the different physicochemical properties of fibrils, the unique preferences of amyloid isoforms in different diseases, and the effect of some mutants. However, the structural polymorphisms also lead to multiple proposed models. Few studies have addressed the relationship between polymorphs and diseases. In other words, it remains unclear which specific polymorph is more related to the disease. Though distinct fibril structures in patients' tissues have been observed, it is not sufficient to exclude the correlation between *in vitro* formed fibrils with diseases. This makes it even more confusing for the structure-based inhibitor design. There are already efforts, such as the work of Goedert and Scheres's team, in which different conditions were tested to reconstruct similar tau (297–391) fibrils as the sample from CTE patients [94]. Their work reveals how different conditions affect tau fibril polymorphism. But further explorations, especially regarding the mechanism of aggregation, are still in need. In addition, the fibril structure of mutants, posttranslationally modified amyloids and condition-induced (like heparin) aggregates reflect some important interactions or processes in aggregation, which may also contribute to the design of inhibitors.

3. Strategies toward structure-based amyloid inhibitors

Rational design is always attractive since it reduces the time and cost of screening. Thanks to the structure determination of amyloids, the rational design of fibril inhibitors becomes possible. Here we devide these structure-based inhibitors into at least four groups (Fig. 2).

3.1. Stabilizing native fold

In view of the involvement and transformational change of amyloid during aggregation, a direct inhibition strategy is to stabilize the free monomers and prevent their aggregation. But as mentioned in our introduction, most amyloidogenic proteins contain IDRs and are unfolded in their native form, which makes it difficult to design an inhibitor binding to free monomers.

In spite of that, a few efforts have pursued on this strategy. Except for the success in transthyretin inhibitors [95] (as transthyretin is natively folded), a recent approach for developing IDP inhibitors has been proposed [96]. In this study, Nath's group developed a repeated simulated annealing (ReSA) technique that mimics the conformation using periodic (every 2 ns) exchanges from a low temperature to high temperature and then back to low temperature. With this technique, they obtained a library containing the conformations of tau4RD segments (244–372) and then analyzed the most frequent and well-resolved 10-residue segments. A docking assay was then applied to these populated segments. After rounds of scoring and comparison, 10 candidates were chosen from 50,000 compounds for experimental testing. ThT fluores-

Table 1
Structures of some amyloid fibrils.

Protein	Length/part	Method	Findings	PDB ID[a]	Resolution (Å)	Year	Ref.
Aβ	1–40	ssNMR	Aβ_{40} polymorph with 2-fold symmetry	2LMN/2LMO	—	2006	[28]
	1–40	ssNMR	Aβ_{40} polymorph with 3-fold symmetry	2LMP/2LMQ	—	2008	[29]
	1–40	ssNMR	ssNMR model of E22Δ Aβ_{40}	2MVX	—	2015	[30]
	1–42	ssNMR	ssNMR model of Aβ_{42}	2MXU	—	2015	[33]
	1–42	ssNMR	ssNMR model of Aβ_{42}	2NAO	—	2016	[31]
	1–42	ssNMR	ssNMR model of Aβ_{42}	5KK3	—	2016	[34]
	1–42	Cryo-EM	Cryo-EM structure of Aβ_{42}	5AEF	7	2015	[39]
	1–42	Cryo-EM	Cryo-EM structure of Aβ_{42}	5OQV	4.0	2017	[40]
	1–40	Cryo-EM	an Aβ_{40} polymorph from patient sample	6SHS	4.5	2019	[41]
	1–42	Cryo-EM	Aβ_{42} polymorphs from patient sample	7Q4B/7Q4M	2.50/2.80	2022	[42]
Tau	fibril in AD	Cryo-EM	tau polymorphs from AD patient sample	5O3L/5O3T	3.4/3.4	2017	[47]
	fibril in AD	Cryo-EM	tau polymorphs from AD patient sample	6HRE/6HRF	3.2/3.3	2018	[48]
	fibril in AD	Cryo-EM	tau polymorphs from AD patient sample	6VI3/6VHL	3.3/3.3	2020	[52]
	fibril in PiD	Cryo-EM	tau polymorphs from PiD patient sample	6GX5	3.2	2018	[49]
	fibril in CTE	Cryo-EM	tau polymorphs from CTE patient sample	6NWP/6NWQ	2.3/3.4	2019	[50]
	fibril in CBD	Cryo-EM	tau polymorphs from CBD patient sample	6TJX/6TJO	3/3.2	2020	[51]
	fibril in CBD	Cryo-EM	tau polymorphs from CBD patient sample	6VHA/6VH7	4.3/3.8	2020	[52]
	2N4R/2N3R	Cryo-EM	structures of heparin-induced tau filaments	6QJH/6QJM/6QJP/6QJQ	3.3/3.3/3.5/3.7	2020	[53]
α-syn	1–140	ssNMR	ssNMR model of α-syn	2N0A	—	2016	[54]
	1–121	Cryo-EM	Cryo-EM structure of α-syn	6H6B/6FLT	3.4/3.42	2018	[57]
	Ac1–140	Cryo-EM	Cryo-EM structure of α-syn (N-terminal acetylated)	6A6B	3.07	2018	[25]
	1–140	Cryo-EM	Cryo-EM structure of α-syn	6CU7/6CU8	3.5/3.6	2018	[58]
	1–140	Cryo-EM	Cryo-EM structure of α-syn	6SST/6SSX/6RT0/6RTB	3.4/2.98/3.10/3.46	2019	[59]
	1–140 E46K	Cryo-EM	Cryo-EM structure of α-syn with E46K mutation	6UFR	2.5	2020	[60]
	1–140 E46K	Cryo-EM	Cryo-EM structure of α-syn with E46K mutation	6L4S	3.37	2020	[61]
	1–140 H50Q	Cryo-EM	Cryo-EM structure of α-syn with H50Q mutation	6PEO/6PES	3.3/3.6	2019	[62]
	1–140 A53T	Cryo-EM	Cryo-EM structure of α-syn with A53T mutation	6LRQ	3.49	2020	[63]
	1–140 pY39	Cryo-EM	Cryo-EM structure of phosphorylated Tyr39 α-syn fibril	6L1T/6L1U	3.22/3.37	2020	[64]
	fibril in MSA	Cryo-EM	α-syn polymorphs from MSA patient sample	6XYO/6XYP/6XYQ	2.60/3.29/3.09	2020	[66]
TDP-43	311–360	Cryo-EM	Cryo-EM structure of TDP-43 segment A (311–360)	6N37/6N3B/6N3A	3.8/3.8/3.3	2019	[71]
	286–331	Cryo-EM	Cryo-EM structure of TDP-43 segment B (286–331 A315E)	6N3C	3.3	2019	[71]
	267–414	Cryo-EM	Cryo-EM structure of entire TDP-43 LCD	7KWZ	3.20	2021	[72]
	fibril in ALS with FTLD	Cryo-EM	Cryo-EM structure of TDP-43 from patient sample	7PY2	2.6	2021	[74]
hIAPP	SUMO-tagged	Cryo-EM	Cryo-EM structure of SUMO-tagged hIAPP	6VW2	3.7	2020	[81]
	1–37-NH_2	Cryo-EM	Cryo-EM structure of C-terminal amidated hIAPP	6Y1A	4.20	2020	[82]
PrP	94–178	Cryo-EM	Cryo-EM structure of human prion (94–178)	6UUR	3.50	2020	[90]
	23–231	Cryo-EM	Cryo-EM structure of full-length human prion	6LNI	2.70	2020	[91]
	23–145	Cryo-EM	Cryo-EM structure of human Y145Stop prion	7RL4	2.86	2021	[92]

[a] DOIs of PDB structures: 10.2210/pdbXXXX/pdb; XXXX is replaced with the PDB ID.

cence assay and intrinsic tyrosine fluorescence were used to analyze the kinetics and relative amount of aggregates in the presence of the candidates among these, one compound was found to delay the aggregation of tau4RD and full-length tau in kinetics. Another similar example was a more previous design of an α-syn inhibitor by Tóth and co-workers [97]. However, the conformation library was randomly selected from NMR studies of α-syn native conformers [98]. Using similar docking steps, finally, they also obtained some hits, but the example in their work only decreased the toxicity of α-syn at the cellular level. Comparing these two studies, it can be found that Nath and co-worker's work used more rational design and expanded the application of the strategy, as their conformation library was generated by an enhanced molecular dynamics method and can be expanded to other IDPs. However, neither of them produced an outstanding inhibition effect, which indicates that this strategy is not mature and needs further optimization. In addition to these efforts on native conformers as docking targets, there are also studies concentrating on the prediction of native folds [99,100]. They combined short-distance crosslink NMR data with molecular dynamics simulations and proposed possible native structures, which may contribute to this strategy in the future.

3.2. Capping inhibitors

The capping strategy was first proposed by Eisenberg's group [101]. This strategy targets the fibril ends. With the help of computational approaches, inhibiting peptides which tightly bind to the end of the steric zipper are designed. If successful, these peptides will block the monomers from joining the existing fibril. To date, several capping inhibitors have been developed. Besides the target proteins, the main difference among these inhibitors is the blocking elements in capping strategy. And we divide them into the following groups according to the blocking segments in their design.

3.2.1. Acetylation and amidation

Although not directly called capping inhibitors, a strategy of developing Aβ inhibitor with docking was proposed by Qiang's group [102]. They chose the ssNMR model of Aβ (PDB 2MPZ, 2LNQ) as targets, and designed initial candidates using a strategy similar to that of Eisenberg's group and performed docking online. Using ThT fluorescence and TEM images as verification, they obtained a few effective candidates (Ac-IGLMV-NH_2, Ac-AIIGLM-NH_2, Ac-IIGLMV-NH_2). These peptides are formed by native residues with acetylation at N-terminus and amidation at C-terminus, which is common in natural organisms. These terminal modifications prevent excess electrostatic interactions which may help elongate the fibril.

3.2.2. D-amino acids

Initially, nonnatural amino acids were used in the inhibitor design of tau segment VQIVYK (residues 306–311) [101]. Eisenberg's group took use of the crystal structure of this tau segment as a template and used Rosetta software to search for possible side-chain conformations of the designed peptide when its β-strand backbone stacks onto the fibril end. Then the Rosetta software was

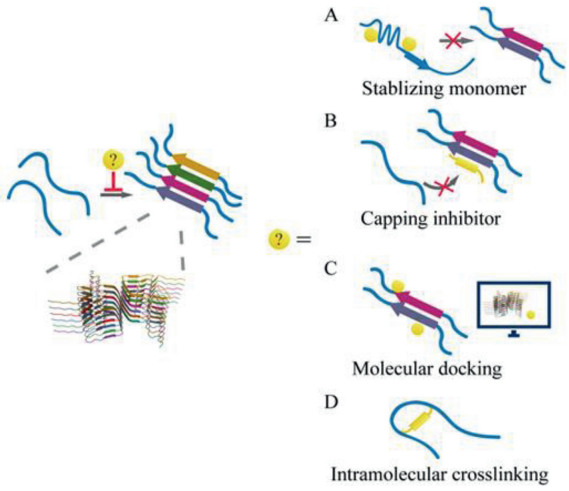

Fig. 2. Some strategies for structure-based amyloid inhibitors (PDB entry of the amyloid structure: 6A6B). (A) The stabilizing strategy in which the inhibitor is designed to stabilize the native fold of amyloids. (B) The capping strategy in which the inhibitors are designed to bind the fibril interface. (C) Molecular dynamic stimulation and docking methods to discover compounds binding to fibrils. (D) The intramolecular crosslinking strategy to prevent aggregation. Image from the RCSB PDB (rcsb.org), PDB entry: 6A6B [25], DOI citation: 10.2210/pdb6a6b/pdb.

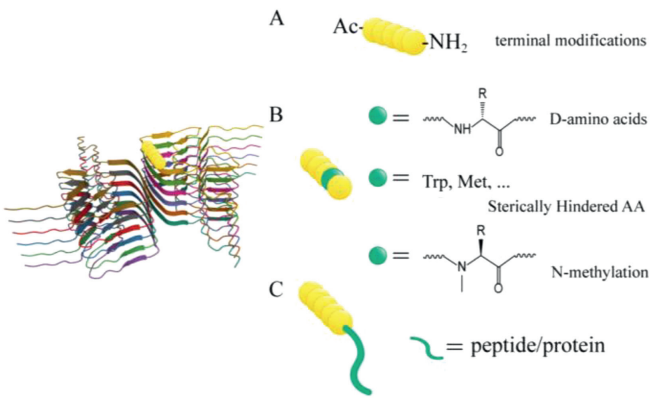

Fig. 3. Capping inhibitors with different blocking elements. The amyloid structure is taken as a model, showing the interface for capping inhibitors (PDB ID: 6A6B). (A) The natural segment used as a blocker. *N*-Acetylation and amidation were also introduced in this strategy. (B) Different blocking elements with unnatural or large hindered residues. (C) Capping inhibitors fused with long peptides or proteins as blockers. Image from the RCSB PDB (rcsb.org), PDB entry: 6A6B [25], DOI citation: 10.2210/pdb6a6b/pdb.

used to calculate and compare the lowest energy of these candidates. Four D-amino-acid peptides were obtained in this research. And they proposed a most effective one, D-TLKIVW, which exhibited inhibition of tau K12 and K19 segments both in ThS fluorescence spectroscopy and electron microscopy.

Then in 2017, they applied this strategy to hIAPP and Aβ. They concentrated on the interaction and similarity between hIAPP 19–29 S20G and Aβ 24–34 [103]. Notably, Aβ 24–34 is not considered as the hydrophobic core segment (KLVFF, residues 16–20), but it is also involved in the core area in ssNMR studies [31,34]. At the beginning of this research, they determined the structure of Aβ 24–34 with microcrystal electron diffraction. This structure showed obvious structural similarity to the hIAPP 19–29 S20G fibril structure identified before [76]. Then they designed 2 capping inhibitors, D-NFEAYFH and D-ELFAHYN in the same approach. These inhibitors successfully inhibited the *in vitro* aggregation of hIAPP and cytotoxicity at the cellular level. Besides, they reduced the toxicity of Aβ_{42} toward N2a cells, which also supported the similarity of the segments in this study.

Another more recent example was provided in 2019 [104]. The familial mutant D23N was the target in this study. The authors found that the Aβ 16–26 containing D23N mutation differs from Aβ 16–20 in structure. It takes a distinct antiparallel form and the β-sheets stack out of register along the fibril axis. They designed capping inhibitors based on this structure. These D-peptides all reduced toxicity and aggregation in N2a cells (IC_{50} < 1 μmol/L) and *in vitro,* respectively. Besides, they found that the cross seeding of tau by Aβ was also inhibited by these inhibitors, indicating that both Aβ and tau are necessary to be targeted in AD therapy.

3.2.3. Residues with large steric hindrance

Some amino acids with large side chains were also used in this strategy. For example, Eisenberg's group designed two capping inhibitors of tau containing bulky side chains [105,106]. In these studies, new segments (275–280 VQIINK, 305–310 SVQIVY) are targeted. They used tryptophan and methionine to substitute the crucial residues in the steric zippers of these fibrils. These designed inhibitors all exhibited inhibitory activity in cells in the studies. In addition, they further tested these inhibitors with patient brain extracts as aggregation seeds [106]. Interestingly, the inhibitors showed different levels of inhibition in brain extracts of different tauopathies (AD, CTE, PSP), and even among different individuals of one disease. This result also suggests polymorphisms involvement in the tauopathies. Despite this variability, the authors obtained a relatively broad-spectrum inhibitor, IN-M4 (DVQMINKKLK), which inhibited tau aggregation in all patient extract samples.

3.2.4. N-Methylation residues

N-Methylation as a backbone modification was reported to interfere with hydrogen bond formation, and thus can be applied to inhibitor design. In 2020, after the identification of hIAPP structure with cryo-EM, Eisenberg's group designed inhibitors according to that structure [81]. All of these inhibitors involve the *N*-methylation in the backbone. Some also contain D-amino acids to block the other filament in the steric zipper whose backbone is in an opposite direction. However, these inhibitors only delayed rather than terminated the aggregation and worked at a high concentration (30 equiv. of hIAPP) in the test.

3.2.5. Long peptides or proteins

Eisenberg's group also used long peptides as capping blocks [107]. In this study, they targeted the NACore of α-syn. In addition to tryptophan substitution or *N*-methylation on this segment, polylysine or TAT peptide was added to increase the solubility. In particular, surface plasmon resonance (SPR) experiments were used as direct evidence of binding to α-syn fibrils in this study. And with other methods, such as ThT fluorescence and YFP-biosensor cells, they demonstrated the effectiveness of these inhibitors.

In addition to Eisenberg's group, Yushchenko and Shvadchak's group also made efforts on this strategy [108–111]. Instead of analyzing the interface, they directly linked a globular protein to α-syn. They hoped to block the fibril ends with this large block and achieved success. They also found that the size of the protein and β-sheets influence the inhibition. Based on this work, a dimer inhibitor was developed in 2019. In addition to the linked globular protein, they used a monomaleimide derivative of sulforhodamine to link two α-syn monomers. They found that this dimer was 5-fold higher in affinity for α-syn fibril ends than the previous inhibitor. By changing the direction of monomers in the dimer, disulfide bond positions and the deleted sequence of α-syn, they obtained an inhibitor with IC_{50} of about 20 nmol/L. Later in

Table 2
Inhibitors based on structural studies.

Category	Target structure (PDB ID*)	Method of target structure	Chemical construction of inhibitor	Year	Ref.
Stabilizing native fold	tau4RD	MD simulation with ReSA	CID1184213 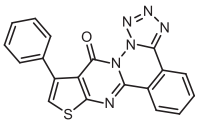	2018	[96]
	α-syn	NMR studies	ELN484228 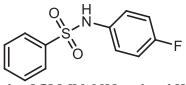	2014	[97]
Capping inhibitors	Aβ_{40} D23N (2MPZ, 2LNQ)	ssNMR	Ac-IGLMV-NH_2, Ac-AIIGLM-NH_2, Ac-IIGLMV-NH_2	2017	[102]
	tau 306-311 (2ON9)	X-ray diffraction	D-TLKIVW	2011	[101]
	Aβ 24-34 (5VOS)	microED	D-NFEAYFH, D-ELFAHYN	2017	[103]
	Aβ 16-26 D23N (6O4J)	microED	D-LYIWVQ, D-LYIWIWRT, D-LYIWIQKT	2019	[104]
	tau 274-283 (5V5B), tau 305-310 (5V5C)	microED	DVQMINKKLK, DVWMINKKRK, SVQWVYE, SVWIWYE,...	2018	[105, 106]
	hIAPP (6VW2)	cryo-EM	NNFGAI$_m$LSS[b], A$_m$ILSSTNVG, NN$_m$FG-GFNN[c] ...	2020	[81]
	α-syn NACore (4RIL)	microED	GAVVWGVTAVKKKKK GAVVWGVTAVGRKKRRQRRRPQ GAVVWGVTAVKKGRKKRRQRRRPQ YGRKKRRQRRRAVVT$_m$GVTAVAE GAVVWGVTAVKKKKK, GAVVWGVTAVGRKKRRQRRRPQ, GAVVWGVTAVKKGRKKRRQRRRPQ, YGRKKRRQRRRAVVTmGVTAVAE	2020	[107]
	α-syn (6CU7, 6CU8)	cryo-EM	T_1R_2-E48C peptide: α-syn (38-78)-α-syn (45-97) with 12aa peptide, GVATVAEKTKEW, linked at E84C through maleimide	2021	[111]
Docking and molecular dynamic simulation	Aβ_{42} (2BEG)	ssNMR	Aminopyrazole trimer derivatives 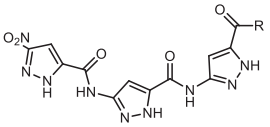	2011	[113]
	Aβ_{40}, Aβ_{42} (2LMN, 2BEG, 2MXU, 2M4J)	ssNMR	Hoechst 34580 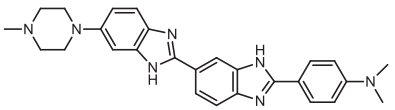 Hoechst 33342 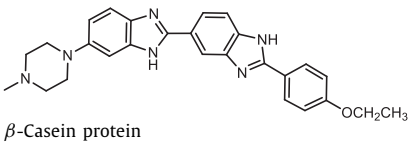	2016	[114]
	Aβ_{42} (2MXU)	ssNMR	β-Casein protein	2018	[116]
	α-syn (2N0A)	ssNMR	Pyridinyltriazole derivatives 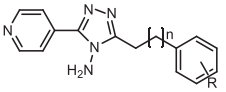	2020	[117]
	hIAPP (3G7V)	X-ray diffraction	Catechins catechins 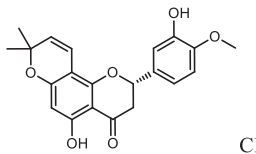 CID636525 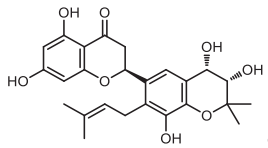 CID44589219 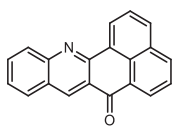 Molport-001-806-035 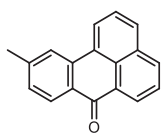 Molport-002-693-913	2017	[118]

(*continued on next page*)

Table 2 (*continued*)

Category	Target structure (PDB ID*)	Method of target structure	Chemical construction of inhibitor	Year	Ref.
Intramolecular crosslinking	hairpin of α-syn 35–56 with AS69 (4BXL)	NMR	β-wrapin protein, AS69	2014, 2019	[120, 121]
	hairpin of α-syn 35–56 with AS69 (4BXL)	NMR	α-syn G41C/V48C, α-synCC	2015, 2020	[122]
	hairpin of α-syn 35–56 with AS69 (4BXL)	NMR	α-synCC fused with α-syn monomer	2020	[123]
	hairpin of IAPP with HI18 (5K5G)	NMR	β-wrapin protein, HI18	2018	[124]

[a] DOIs of PDB structures: 10.2210/pdbXXXX/pdb; XXXX is replaced with the PDB ID.
[b] The subscript "m" indicates the residue after this subscript is N-methylated at its backbone.
[c] The underlined "FNN" stands for D-FNN.

2020, they further discussed the influences of the sequence of α-syn monomer, and the charge, size, and secondary structure of the fused globular protein in detail. Fairly, this series of work yielded efficient inhibitors of α-syn with such low IC_{50}, but the difficulties when applying these large protein inhibitors to therapeutics or even cells seem to be predictable. However, they have just reported similar inhibitors partially overcoming this problem [111]. Protein inhibitors for different polymorphs referring to the cryo-EM data of α-syn (PDB 6CU7/6CU8) [58] were designed among these inhibitors, an optimized inhibitor, T_1R_2-E48C-pep, which binds to both the "rod" polymorph and the "twister" polymorph and is linked to a 12aa peptide on the E48C mutant site, showed great efficiency. The IC_{50} of it can be as low as about 5 nmol/L. And it can penetrate cells and selectively bind to α-syn, which make it a potential candidate for clinical use if its permeability across blood−brain barrier is further improved.

3.3. Other docking and molecular dynamic simulation strategies

Before being applied to amyloid inhibitors, the docking and molecular dynamic simulation of compounds with target proteins have been widely used in medical research [112]. But to some extent, they are often only used as complementary methods in mechanistic studies of drugs. However, in some studies they were also used to find hits from a series of designed molecules. A common case starts with the reported inhibitors. A library of the analogues will be constructed, and docked with the target. The *in silico* process will produce several candidates. Then after validation with wet-lab methods, some potential hits will be found. A series of new compounds have been found in this way, covering Aβ [113–116], α-syn [117], hIAPP [118], and other amyloids [119]. However, these optimized compounds are usually similar to the existing inhibitors, and are therefore difficult to overcome the associated problems, such as solubility and selectivity.

3.4. Intramolecular crosslinking strategy

Another category of inhibitors was designed to avoid β-sheets in amyloids. These designs start with unique intramolecular hairpin structures. In 2014, Hoyer's group designed a protein inhibitor binding to α-syn [120]. This β-wrapin protein, AS69, was able to bind to the β1 and β2 regions of α-syn and maintain a hairpin structure of this region. Basing on this study, in 2019, Hoyer's group performed more detailed research on this molecule [121]. They found that it is AS69-α-syn complex that exhibits efficient inhibition of the secondary nucleation process. Thus the AS69 showed two roles in stabilizing monomers and forming AS69-α-syn complex as an inhibitor to prevent secondary nucleation.

Hoyers group also explored a covalently linked α-syn hairpin inhibitor [122]. They introduced two cysteine mutants G41C/V48C to α-syn. The disulfide bond formed between these two residues restricted these regions to a hairpin state. This structure may interact with some species in the aggregation process, such as oligomer and fibril ends, then inhibit aggregation. In 2020, they further explored the mechanism and optimized this inhibitor [123]. This inhibitor can inhibit aggregation both by forming an inhibitor-fibril complex as a competitive inhibitor and by attracting monomers to this complex as an uncompetitive inhibitor. Inspired by this finding, they designed inhibitor-monomer fusion constructs. And this new inhibitor has lower IC_{50} of approximately 11 nmol/L.

In addition to α-syn, the hairpin structure was also effective for the inhibition of hIAPP and Aβ [124]. The starting point for these studies was using hairpin structures to avoid β-sheets in amyloids, which is more similar to β-sheet breakers. Actually, the hairpin structures have been used as β-sheet breakers in some studies [125,126].

Here we have summarized some rational strategies of structure-based amyloid inhibitors (Table 2). Notably, the aid of computers is widely used in these strategies, as with complicated structural details, it is almost impossible to optimize the binding affinity to targets only in mind.

Besides, a large portion of these inhibitors mainly target the core of fibril aggregation. This may come from the importance of the core regions and the defined structure of these regions. However, the flanking region which is usually involved in the "fuzzy coat" of the fibril structure may also play important roles, and be valuable for targeting [127].

Some readers may also notice that the common "β-sheet breaker peptides" [128–130] with similar sequences to some regions of amyloids are not included in the catalogue above. This is mainly because these strategies are based on the amyloid sequences and only introduce β-sheet breaking residues or modifications. The design of these studies did not refer to the structural studies of amyloid, even though some of them gave the combined structure of inhibitors and aggregates in their articles.

4. Summary and perspective

Amyloid misfolding and aggregation correlate with many diseases. And the aggregation process of amyloid fibrils is a target in these diseases. In recent years, progress in analysis techniques, such as ssNMR and cryo-EM has led to many high-resolution structures of amyloid fibrils. These fibrils show extensive polymorphism and provided some important information explaining certain phenomena in the structure sights.

In addition, we introduced some rationally designed inhibitors. These inhibitors are designed based on structural studies of amyloid proteins. Some of these studies provided potential inhibitors with improved efficacy. In spite of such studies, some things should be noted. Most importantly, the pathogenesis of most amyloidosis is not clear. Thus, whether targeting amyloid aggregation is a good strategy remains unknown. There are also other trials

in medical research, such as immunotherapy [131] and nanotherapeutic approaches [132]. In addition, as mentioned above, the inhibitors at present primarily target the fibril core despite that other regions also influence aggregation and can be modulated. In summary, these studies presented not only potential inhibitor hits but also abundant information that benefits our understanding of amyloid diseases. And it is predictable that these high-resolution structures will help the design of novel inhibitors.

Declaration of competing interest

The authors declare that they have no known competing financial interests or personal relationships that could have appeared to influence the work reported in this paper.

Acknowledgments

Support from the National Key R&D Program of China (Nos. 2018YFA0507600, 2019YFA0904200) and the National Natural Science Foundation of China (No. 92053108) is gratefully acknowledged.

References

[1] F. Chiti, C.M. Dobson, Annu. Rev. Biochem. 86 (2017) 27–68.
[2] I. Benilova, E. Karran, B. De Strooper, Nat. Neurosci. 15 (2012) 349–357.
[3] K. Tepper, J. Biernat, S. Kumar, et al., J. Biol. Chem. 289 (2014) 34389–34407.
[4] H.A. Lashuel, C.R. Overk, A. Oueslati, et al., Nat. Rev. Neurosci. 14 (2013) 38–48.
[5] G. Li, Y.M. Li, Prog. Chem. 32 (2020) 14–22.
[6] K.W. Tipping, P. van Oosten-Hawle, E.W. Hewitt, et al., Trends Biochem. Sci. 40 (2015) 719–727.
[7] M. Goedert, D.S. Eisenberg, R.A. Crowther, Annu. Rev. Neurosci. 40 (2017) 189–210.
[8] M. Hasegawa, T. Nonaka, M. Masuda-Suzukake, Pharmacol. Ther. 172 (2017) 22–33.
[9] X. Mao, M.T. Ou, S.S. Karuppagounder, et al., Science 353 (2016) aah3374.
[10] M.R. Ma, Z.W. Hu, Y.F. Zhao, et al., Sci. Rep. 6 (2016) 37130.
[11] Q.Q. Li, Y.Q. Liu, Y.Y. Luo, et al., Chem. Commun. 56 (2020) 5370–5373.
[12] Y.S. Eisele, C. Monteiro, C. Fearns, et al., Nat. Rev. Drug Discov. 14 (2015) 759–780.
[13] Q.Q. Li, T.T. Chu, Y.X. Chen, et al., Chin. J. Chem. 32 (2014) 964–968.
[14] A. Paul, B.D. Zhang, S. Mohapatra, et al., Front. Mol. Biosci. 6 (2019) 16.
[15] L. Urquhart, Nat. Rev. Drug Discov. 18 (2019) 575.
[16] G. Li, W.Y. Yang, W.H. Li, et al., Chemistry 26 (2020) 3499–3503.
[17] P. Maiti, G.L. Dunbar, Int. J. Mol. Sci. 19 (2018) 1637.
[18] W.H. Ji, Z.B. Xiao, G.Y. Liu, et al., Chin. Chem. Lett. 28 (2017) 1829–1834.
[19] V. Armiento, A. Spanopoulou, A. Kapurniotu, Angew. Chem. Int. Ed. 59 (2020) 3372–3384.
[20] D.S. Eisenberg, M.R. Sawaya, Annu. Rev. Biochem. 86 (2017) 69–95.
[21] D. Li, C. Liu, Biochemistry 59 (2020) 639–646.
[22] R. Tycko, Annu. Rev. Phys. Chem. 62 (2011) 279–299.
[23] X.C. Bai, G. McMullan, S.H. Scheres, Trends Biochem. Sci. 40 (2015) 49–57.
[24] J.P. Renaud, A. Chari, C. Ciferri, et al., Nat. Rev. Drug Discov. 17 (2018) 471–492.
[25] Y. Li, C. Zhao, F. Luo, et al., Cell Res. 28 (2018) 897–903.
[26] T. Qiu, Q. Liu, Y.X. Chen, et al., J. Pept. Sci. 21 (2015) 522–529.
[27] A.T. Petkova, R.D. Leapman, Z. Guo, et al., Science 307 (2005) 262–265.
[28] A.T. Petkova, W.M. Yau, R. Tycko, Biochemistry 45 (2006) 498–512.
[29] A.K. Paravastu, R.D. Leapman, W.M. Yau, et al., Proc. Natl. Acad. Sci. U. S. A. 105 (2008) 18349–18354.
[30] A.K. Schutz, T. Vagt, M. Huber, et al., Angew. Chem. Int. Ed. 54 (2015) 331–335.
[31] M.A. Walti, F. Ravotti, H. Arai, et al., Proc. Natl. Acad. Sci. U. S. A. 113 (2016) E4976–E4984.
[32] L. Jin, W.H. Wu, Q.Y. Li, et al., Nanoscale 3 (2011) 4746–4751.
[33] Y. Xiao, B. Ma, D. McElheny, et al., Nat. Struct. Mol. Biol. 22 (2015) 499–505.
[34] M.T. Colvin, R. Silvers, Q.Z. Ni, et al., J. Am. Chem. Soc. 138 (2016) 9663–9674.
[35] C. Sachse, C. Xu, K. Wieligmann, et al., J. Mol. Biol. 362 (2006) 347–354.
[36] C. Sachse, M. Fandrich, N. Grigorieff, Proc. Natl. Acad. Sci. U. S. A. 105 (2008) 7462–7466.
[37] M. Schmidt, C. Sachse, W. Richter, et al., Proc. Natl. Acad. Sci. U. S. A. 106 (2009) 19813–19818.
[38] R. Zhang, X. Hu, H. Khant, et al., Proc. Natl. Acad. Sci. U. S. A. 106 (2009) 4653–4658.
[39] M. Schmidt, A. Rohou, K. Lasker, et al., Proc. Natl. Acad. Sci. U. S. A. 112 (2015) 11858–11863.
[40] L. Gremer, D. Scholzel, C. Schenk, et al., Science 358 (2017) 116–119.
[41] M. Kollmer, W. Close, L. Funk, et al., Nat. Commun. 10 (2019) 4760.
[42] Y. Yang, D. Arseni, W. Zhang, et al., Science 375 (2022) 167–172.
[43] M.R. Sawaya, S. Sambashivan, R. Nelson, et al., Nature 447 (2007) 453–457.
[44] A. Savastano, G. Jaipuria, L. Andreas, et al., Sci. Rep. 10 (2020) 21210.
[45] O.C. Andronesi, M. von Bergen, J. Biernat, et al., J. Am. Chem. Soc. 130 (2008) 5922–5928.
[46] V. Daebel, S. Chinnathambi, J. Biernat, et al., J. Am. Chem. Soc. 134 (2012) 13982–13989.
[47] A.W.P. Fitzpatrick, B. Falcon, S. He, et al., Nature 547 (2017) 185–190.
[48] B. Falcon, W. Zhang, M. Schweighauser, et al., Acta Neuropathol. 136 (2018) 699–708.
[49] B. Falcon, W. Zhang, A.G. Murzin, et al., Nature 561 (2018) 137–140.
[50] B. Falcon, J. Zivanov, W. Zhang, et al., Nature 568 (2019) 420–423.
[51] W. Zhang, A. Tarutani, K.L. Newell, et al., Nature 580 (2020) 283–287.
[52] T. Arakhamia, C.E. Lee, Y. Carlomagno, et al., Cell 180 (2020) 633–644.e12.
[53] W. Zhang, B. Falcon, A.G. Murzin, et al., eLife 8 (2019) e43584.
[54] M.D. Tuttle, G. Comellas, A.J. Nieuwkoop, et al., Nat. Struct. Mol. Biol. 23 (2016) 409–415.
[55] G. Lv, A. Kumar, K. Giller, et al., J. Mol. Biol. 420 (2012) 99–111.
[56] J. Verasdonck, L. Bousset, J. Gath, et al., Biomol. NMR Assign. 10 (2016) 5–12.
[57] R. Guerrero-Ferreira, N.M. Taylor, D. Mona, et al., eLife 7 (2018) e36402.
[58] B. Li, P. Ge, K.A. Murray, et al., Nat. Commun. 9 (2018) 3609.
[59] R. Guerrero-Ferreira, N.M. Taylor, A.A. Arteni, et al., eLife 8 (2019) e48907.
[60] D.R. Boyer, B. Li, C. Sun, et al., Proc. Natl. Acad. Sci. U. S. A. 117 (2020) 3592–3602.
[61] K. Zhao, Y. Li, Z. Liu, et al., Nat. Commun. 11 (2020) 2643.
[62] D.R. Boyer, B. Li, C. Sun, et al., Nat. Struct. Mol. Biol. 26 (2019) 1044–1052.
[63] Y. Sun, S. Hou, K. Zhao, et al., Cell Res. 30 (2020) 360–362.
[64] K. Zhao, Y.J. Lim, Z. Liu, et al., Proc. Natl. Acad. Sci. U. S. A. 117 (2020) 20305–20315.
[65] S. Zhang, Y.Q. Liu, C. Jia, et al., Proc. Natl. Acad. Sci. U. S. A. 118 (2021) e2011196118.
[66] M. Schweighauser, Y. Shi, A. Tarutani, et al., Nature 585 (2020) 464–469.
[67] Y.S. Fang, K.J. Tsai, Y.J. Chang, et al., Nat. Commun. 5 (2014) 4824.
[68] E.B. Lee, V.M. Lee, J.Q. Trojanowski, Nat. Rev. Neurosci. 13 (2011) 38–50.
[69] E.L. Guenther, Q. Cao, H. Trinh, et al., Nat. Struct. Mol. Biol. 25 (2018) 463–471.
[70] Z. Chang, J. Deng, W. Zhao, et al., Biochem. Biophys. Res. Commun. 532 (2020) 655–661.
[71] Q. Cao, D.R. Boyer, M.R. Sawaya, et al., Nat. Struct. Mol. Biol. 26 (2019) 619–627.
[72] Q. Li, W.M. Babinchak, W.K. Surewicz, Nat. Commun. 12 (2021) 1620.
[73] J. Shenoy, N. El Mammeri, A. Dutour, et al., FEBS J. 287 (2020) 2449–2467.
[74] D. Arseni, M. Hasegawa, A.G. Murzin, et al., Nature 601 (2022) 139–143.
[75] E.H. Pilkington, E.N. Gurzov, A. Kakinen, et al., Sci. Rep. 6 (2016) 21274.
[76] P. Krotee, J.A. Rodriguez, M.R. Sawaya, et al., eLife 6 (2017) e19273.
[77] C.A. Jurgens, M.N. Toukatly, C.L. Fligner, et al., Am. J. Pathol. 178 (2011) 2632–2640.
[78] P. Liu, S. Zhang, M.S. Chen, et al., Chem. Commun. 48 (2012) 191–193.
[79] S. Luca, W.M. Yau, R. Leapman, et al., Biochemistry 46 (2007) 13505–13522.
[80] S. Bedrood, Y. Li, J.M. Isas, et al., J. Biol. Chem. 287 (2012) 5235–5241.
[81] Q. Cao, D.R. Boyer, M.R. Sawaya, et al., Nat. Struct. Mol. Biol. 27 (2020) 653–659.
[82] C. Roder, T. Kupreichyk, L. Gremer, et al., Nat. Struct. Mol. Biol. 27 (2020) 660–667.
[83] M.E. Oskarsson, J.F. Paulsson, S.W. Schultz, et al., Am. J. Pathol. 185 (2015) 834–846.
[84] C. Scheckel, A. Aguzzi, Nat. Rev. Genet. 19 (2018) 405–418.
[85] R. Riek, S. Hornemann, G. Wider, et al., Nature 382 (1996) 180–182.
[86] J.J. Helmus, K. Surewicz, P.S. Nadaud, et al., Proc. Natl. Acad. Sci. U. S. A. 105 (2008) 6284–6289.
[87] J.J. Helmus, K. Surewicz, W.K. Surewicz, et al., J. Am. Chem. Soc. 132 (2010) 2393–2403.
[88] T. Theint, P.S. Nadaud, D. Aucoin, et al., Nat. Commun. 8 (2017) 753.
[89] D. Aucoin, Y. Xia, T. Theint, et al., J. Struct. Biol. 206 (2019) 36–42.
[90] C. Glynn, M.R. Sawaya, P. Ge, et al., Nat. Struct. Mol. Biol. 27 (2020) 417–423.
[91] L.Q. Wang, K. Zhao, H.Y. Yuan, et al., Nat. Struct. Mol. Biol. 27 (2020) 598–602.
[92] Q. Li, C.P. Jaroniec, W.K. Surewicz, bioRxiv (2021), 10.1101/2021.08.10.455830.
[93] J.K. Choi, I. Cali, K. Surewicz, et al., Proc. Natl. Acad. Sci. U. S. A. 113 (2016) 13851–13856.
[94] S. Lovestam, F.A. Koh, B. van Knippenberg, et al., eLife 11 (2022) e76494.
[95] T. Yokoyama, M. Mizuguchi, J. Med. Chem. 63 (2020) 14228–14242.
[96] D.W. Baggett, A. Nath, Biochemistry 57 (2018) 6099–6107.
[97] G. Toth, S.J. Gardai, W. Zago, et al., PLoS One 9 (2014) e87133.
[98] M.M. Dedmon, K. Lindorff-Larsen, J. Christodoulou, et al., J. Am. Chem. Soc. 127 (2005) 476–477.
[99] N.I. Brodie, K.I. Popov, E.V. Petrotchenko, et al., PLoS Comput. Biol. 15 (2019) e1006859.
[100] K.I. Popov, K.A.T. Makepeace, E.V. Petrotchenko, et al., Structure 27 (2019) 1710–1715 e4.
[101] S.A. Sievers, J. Karanicolas, H.W. Chang, et al., Nature 475 (2011) 96–100.
[102] Q. Cheng, W. Qiang, J. Phys. Chem. B 121 (2017) 5544–5552.
[103] P. Krotee, S.L. Griner, M.R. Sawaya, et al., J. Biol. Chem. 293 (2018) 2888–2902.
[104] S.L. Griner, P. Seidler, J. Bowler, et al., eLife 8 (2019) e46924.
[105] P.M. Seidler, D.R. Boyer, J.A. Rodriguez, et al., Nat. Chem. 10 (2018) 170–176.
[106] P.M. Seidler, D.R. Boyer, K.A. Murray, et al., J. Biol. Chem. 294 (2019) 16451–16464.
[107] S. Sangwan, S. Sahay, K.A. Murray, et al., eLife 9 (2020) e46775.

[108] V.V. Shvadchak, K. Afitska, D.A. Yushchenko, Angew. Chem. Int. Ed. 57 (2018) 5690–5694.
[109] Y.A. Kyriukha, K. Afitska, A.S. Kurochka, et al., J. Med. Chem. 62 (2019) 10342–10351.
[110] K. Afitska, A. Priss, D.A. Yushchenko, et al., J. Mol. Biol. 432 (2020) 967–977.
[111] A. Priss, K. Afitska, M. Galkin, et al., J. Med. Chem. 64 (2021) 6827–6837.
[112] S. Vilar, G. Cozza, S. Moro, Curr. Top. Med. Chem. 8 (2008) 1555–1572.
[113] K. Hochdorffer, J. Marz-Berberich, L. Nagel-Steger, et al., J. Am. Chem. Soc. 133 (2011) 4348–4358.
[114] N.Q. Thai, N.H. Tseng, M.T. Vu, et al., J. Comput. Aided Mol. Des. 30 (2016) 639–650.
[115] A. Espargaro, T. Ginex, M.D. Vadell, et al., J. Nat. Prod. 80 (2017) 278–289.
[116] S. Hojati, A. Ghahghaei, M. Lagzian, J. Biomol. Struct. Dyn. 36 (2018) 2118–2130.
[117] S. Vittorio, I. Adornato, R. Gitto, et al., J. Enzym. Inhib. Med. Chem. 35 (2020) 1727–1735.
[118] P. Patel, K. Parmar, V.K. Vyas, et al., J. Mol. Graph. Model. 77 (2017) 295–310.
[119] J.H. Zhao, H.L. Liu, P. Elumalai, et al., J. Mol. Model. 19 (2013) 151–162.
[120] E.A. Mirecka, H. Shaykhalishahi, A. Gauhar, et al., Angew. Chem. Int. Ed. 53 (2014) 4227–4230.
[121] E.D. Agerschou, P. Flagmeier, T. Saridaki, et al., eLife 8 (2019) e46112.
[122] H. Shaykhalishahi, A. Gauhar, M.M. Wordehoff, et al., Angew. Chem. Int. Ed. 54 (2015) 8837–8840.
[123] E.D. Agerschou, V. Borgmann, M.M. Wordehoff, et al., Chem. Sci. 11 (2020) 11331–11337.
[124] A.A. Orr, H. Shaykhalishahi, E.A. Mirecka, et al., Comput. Chem. Eng. 116 (2018) 322–332.
[125] A. Jha, M.G. Kumar, H.N. Gopi, et al., Langmuir 34 (2018) 1591–1600.
[126] N. Ghosh, L.M. Kundu, Bioorg. Med. Chem. 33 (2021) 116017.
[127] S.M. Ulamec, D.J. Brockwell, S.E. Radford, Front. Neurosci. 14 (2020) 611285.
[128] S. Bieler, C. Soto, Curr. Drug Targets 5 (2004) 553–558.
[129] A. Francioso, P. Punzi, A. Boffi, et al., Bioorg. Med. Chem. 23 (2015) 1671–1683.
[130] P. Yang, C. Yang, K. Zhang, et al., Chin. Chem. Lett. 29 (2018) 1811–1814.
[131] S. Kwon, M. Iba, C. Kim, et al., Neurotherapeutics 17 (2020) 935–954.
[132] H. Zeng, Y. Qi, Z. Zhang, et al., Chin. Chem. Lett. 32 (2021) 1857–1868.